Materials Today Nano 23 (2023) 100359

Contents lists available at ScienceDirect

Materials Today Nano

journal homepage: https://www.evise.com/profile/#/MTNANO/login

Ultrathin breathable and stretchable electronics based on patterned nanofiber composite network

J. Li [a, b, 1], X. Pan [a, d, 1], Y. Zhang [a, b], Y. Liu [a, b], C. Wang [a, c], Y. Wan [a, b], J. Tao [a, c], R. Bao [a, b, d, **], C. Pan [a, b, d, *]

[a] CAS Center for Excellence in Nanoscience, Beijing Key Laboratory of Micro-nano Energy and Sensor, Beijing Institute of Nanoenergy and Nanosystems, Chinese Academy of Sciences, Beijing, 101400, PR China
[b] School of Nanoscience and Engineering, University of Chinese Academy of Sciences, Beijing, 100049, PR China
[c] College of Physics and Optoelectronic Engineering, Shenzhen University, Shenzhen, 518060, China
[d] Center on Nanoenergy Research, School of Physical Science and Technology, Guangxi University, Nanning, Guangxi, 530004, PR China

ARTICLE INFO

Article history:
Received 17 January 2023
Received in revised form
4 May 2023
Accepted 2 June 2023
Available online 14 June 2023

Keywords::
Patterned electrospinning
Stretchable electrode
Strain sensor
Nanofibers

ABSTRACT

Wearable comfort and performance modulation of stretchable electronics are the focus of next-generation electronic skin. Herein, we developed ultrathin breathable and stretchable electronics by introducing elaborate patterned electrospinning technology. The principle of patterned electrospinning technology is studied, and this technology is proved to be universal for variety of polymers experimentally. The effect of electrospinning time and patterned pore size on the performance of patterned electrospun film is studied. Using an ultrathin patterned stretchable thermoplastic polyurethane electrospun film (10 μm) as a supportive layer, a patterned nanofiber composite network is constructed, combined with Ag nanowires and thermoplastic polyurethane/Ag nanofibers. The patterned nanofiber composite network is achieved with outstanding stretchability and conductivity, while the mean sheet resistance is as low as 1.59 Ω/sq and can be stretched to 110% strain. The electromechanical performance of nanofiber composite network is controlled by the pore size of patterned electrospun film, which can be applied for stable, breathable, and stretchable electrode and strain sensor. Hence, the elaborate patterned electrospinning technology and the fabrication and modulation of patterned nanofiber composite network offer a method for stretchable electronics.

1. Introduction

With the rapid development of Internet of Things technology and electronic skin, the research on flexible electronics, including flexible sensors and flexible electrodes, is of great significance [1–3]. Among flexible electronics, stretchable electronics can maintain good conformal contact with the skin even while the skin is being stretched or contracted, realizing the effective sensing of the external stimulation on the skin and maintaining stable connection with electrode. Researchers have developed stretchable electronics by embedding conductive materials into stretchable polymers [4,5]. Recently, the main methods of preparing conductive materials for stretchable circuits include direct-write extrusion [6–8], microcontact printing [9], inkjet printing [10,11], masked deposition [12,13], and so on. However, this kind of stretchable electronics is not breathable and is unable to release the sweat of human skin in time, which may cause the delamination of stretchable electronics from the skin and cause inflammation. Moreover, this kind of stretchable electronics faces the contradiction between high conductivity and easy agglomeration and high elastic modulus and easy fracture [14,15]. Therefore, developing breathable and stretchable electronics with high conductivity and elastic modulus similar to that of the skin is the key to realizing robust sensing function and wearing comfort.

To ensure a stable signal response during use, stretchable electronics must form good conformal contact with complex surfaces such as the skin. Two current methods for achieving this are three-dimensional printing and ultrathin materials. Three-dimensional printing allows for the direct preparation of free-form functional devices on complex geometric surfaces, making it a popular

* Corresponding author.
** Corresponding author.
E-mail addresses: baorongrong@binn.cas.cn (R. Bao), cfpan@binn.cas.cn (C. Pan).
[1] Authors contributed equally to this work.

https://doi.org/10.1016/j.mtnano.2023.100359
2588-8420/

research topic [16,17]. However, it has limitations such as relying on open-loop calibration and complicated procedures, which restrict its application to prepare stretchable electronics [18]. An alternative method involves fabricating a flat device with thin, deformable materials through microfabrication and then transferring it to the target surface for a conformal interface [19]. This approach is simple to operate and does not require complex instruments, making it an effective way to achieve conformal contact. As a result, it has gained popularity due to its advantages over other methods. At present, breathable flexible electronics usually use nanofiber film as substrate or template, metal nanowire or film, graphene and so on as conductive functional materials, possessing good flexibility, conductivity, and stability in general [14,20–24]. Introduction of breathability allows human skin breathing and sweating freely and can improve the comfort and safety of the long-term use of flexible electronics, avoiding the skin inflammation resulting from the impermeability [25]. The present breathable and stretchable electronics mainly focus on the innovation of the materials of stretchable substrate [26,27] or the materials and the preparation technology of conductive layer [21,28,29]. Realizing the optimization of the structure of stretchable substrate can further achieve the modulation of performance of stretchable electronics, expanding the application of the breathable and stretchable electronics in the fields of wearable devices and human-machine interaction.

In general, patterned electrospun films possess higher porosity and breathability, better stretchability, and adjustable elastic modulus [30,31], commonly applied for air filtration devices [30] or as “antibacterial gauze” to accelerate wound healing in the medical field [32,33]. Utilizing patterned conductive or insulated collectors as the negative electrode for electrospinning can make the potential near the collector fluctuate orderly in the electrospinning process, which is pivotal for achieving patterned electrospinning [34,35]. The common patterned collectors are wire mesh [36,37], conducting protrusion [34,38], topological non-conductive collectors [39], etc. Furthermore, achieving controllable fabrication of patterned electrospinning in a sophisticated manner, so as to realize the accurate regulation of Young's modulus of electrospinning film, is of great significance for the study of stretchable electronics.

Here, we exploit the delicate patterned electrospinning technology via micromachining technology and realize the modulation of Young's modulus of nanofiber film, thus achieving the performance modulation of breathable and stretchable electronics. A breathable and stretchable stable electrode and a highly sensitive tactile sensor were developed. Firstly, the technology and principle of patterned electrospun film, prepared by micromachining technology were studied, and the universality of patterned electrospinning technology for a variety of polymers was proven experimentally. The effect of electrospinning time on the pore size of patterned films was further studied, and the mechanical properties of patterned electrospun films were controlled by adjusting the pore size. Patterned nanofiber composite network (PNCN), consisting of silver nanowires (Ag NWs), patterned electrospun thermoplastic polyurethane-Ag nanofibers (TPU-Ag NFs), were prepared by vacuum filtration and magnetron sputtering. The mean sheet resistance is as low as 1.59 Ω/sq. The electromechanical properties of PNCN can be modulated by the Young's modulus of patterned electrospun film, and PNCNs achieve a better breathability than commercial cotton. A breathable and stretchable tactile sensor with gauge factor (GF) up to 88 in the strain range of 79% is achieved, as well as a breathable and stretchable stable electrode with good conductivity is achieved even being stretched to 110% strain. The patterned electrospinning technology and the fabrication of PNCN provide a new method for novel stretchable electronics.

2. Results and discussion

One of the greatest merits of stretchable electronics is its ability of being extremely conformal to human skin, ensuring good deformability with the skin. As shown in Fig. 1(a), PNCN can achieve stretchability with porous structure by introducing patterned electrospinning technology. Transferring PNCN on human skin and corresponding photographs are shown in the inset of Fig. 1(a). PNCNs contact tightly with human skin, and the ultrathin property (10 μm) makes the PNCN fit within the wrinkle of skin. The enlarged photograph shows the micropores of PNCN, which are beneficial for breathability and the performance modulation of PNCN. Resulting from contrivable stretchability, the PNCN can still keep close contact with the hand skin while being squeezed or stretched.

The schematic illustration of the fabrication process of PNCN using the flexible patterned collector is shown in Fig. 1(b). First, fabricate patterned TPU NF film by electrospinning using patterned collectors with a regular hexagonal array pattern, which is fabricated by micromachining technology. Then, construct Ag NWs on patterned TPU NF film through vacuum filtration. Lastly, achieve PNCN by magnetron sputtering Ag films on the Ag NWs-TPU NFs network, the detailed fabrication process is shown in the Experimental Section and Fig. S2. The scanning electron microscopy (SEM) images of PNCN and enlarged view are shown in Fig. 1(c); the pattern of PNCN is closer to round, and the TPU NFs inside the circle are relatively sparse than the TPU NFs outside the circle, which reveal the patterning of electrospinning films. The enlarged SEM images of PNCN show that the PNCN is constructed on the patterned TPU NF film. It is worth noting that the Ag NWs used in PNCN are of high aspect ratio, as shown in Fig. S1, with a diameter of 50 nm and a length of 100 μm. Ag NWs with high aspect ratio usually possess excellent flexibility and are not easy to fracture under strain, so they can maintain good conductivity [14]. The sheet resistance of PNCN was measured by four-probe method, and the average sheet resistance is as low as 1.59 Ω/sq. The cross-sectional SEM images of PNCN are shown in figure S3, and Ag NWs exist on the surface, inside, and even at the bottom of the PNCN, which explains the low resistance of the PNCN. It can be seen from Fig. S3(c) that Ag NWs are closely interweaved with the TPU NFs, which ensures that Ag NWs and TPU NFs are less able to slide when the PNCN is being stretched and can maintain a relatively stable conductivity. Fig. S3(d) shows a schematic diagram of the PNCN cross-section, which can more clearly demonstrate the Ag NWs interwoven with the TPU NFs.

The principle of patterned electrospinning is simulated and analyzed by the electrical module of COMSOL software. Detailed simulation parameters are shown in SI. The simulation results are shown in Fig. 1(d). The potential is highest near the electrospinning needle and the lowest near the collector. Compared to flat collector, the electric field distribution at the patterned collector becomes non-uniform, and the degree of non-uniformity decreases with the decreasing of the hole size (Fig. S4(a)). The potential distributions along the X direction of the needle and the Y direction of the collector were derived and plotted. As shown in Fig. 1(e), compared to the flat collector, the potential near the patterned collector becomes orderly undulating, while the positively charged electrospun droplets tend to concentrate on the Ag film with lower potential, so that patterned electrospun films can be obtained. The potential along the X direction of the electrospinning needle is relatively high compared to that along the flat collector, which can accelerate the droplet ejection from the Taylor cone [40]. In addition, with the decrease in pore size, the amplitude of potential fluctuation gradually decreases, as shown in Figs. S4(a) and (b). The potential near the collector of the macropore fluctuates between - 790 V and -

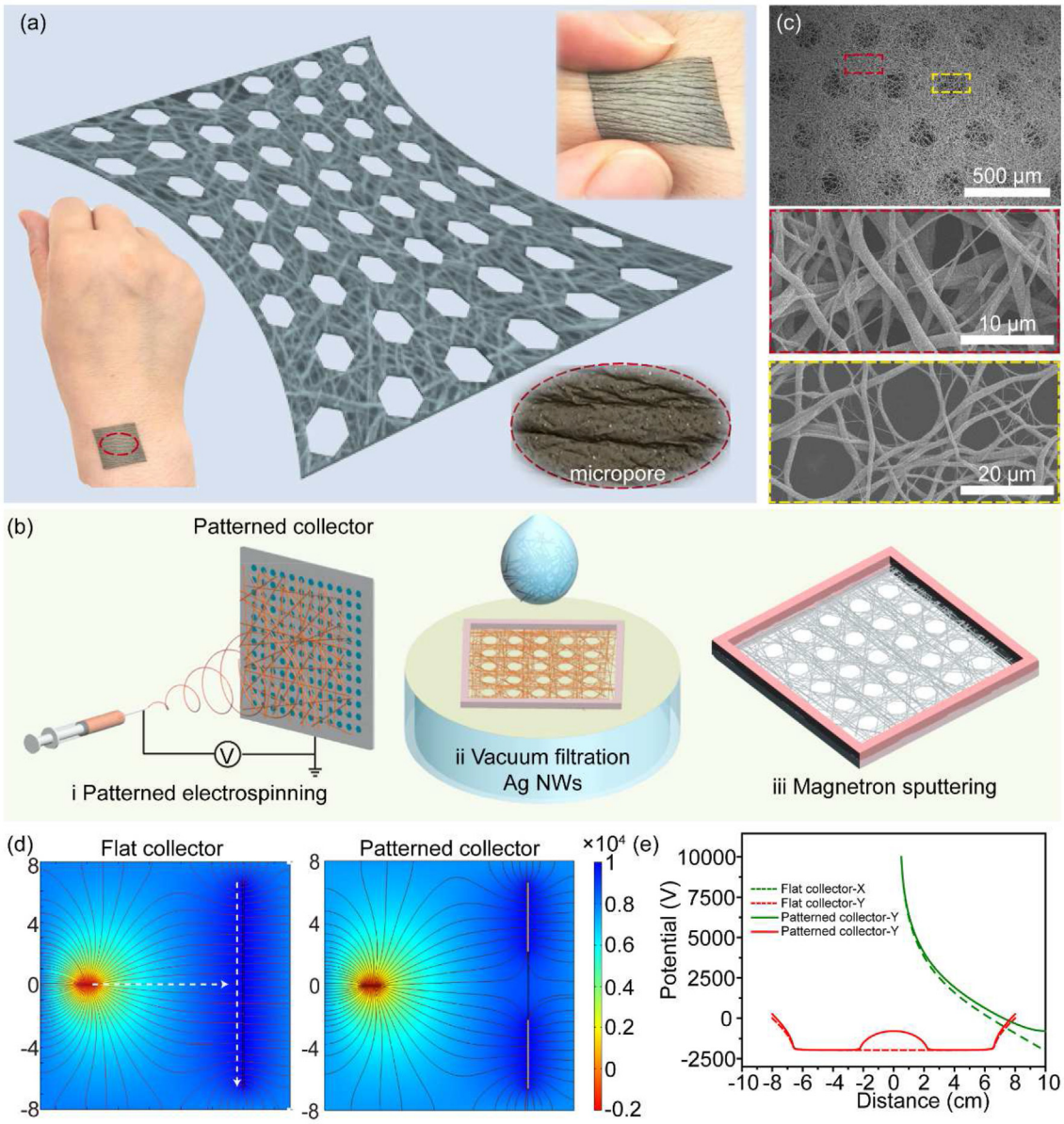

Fig. 1. Fabrication process, characterization, and theoretical analysis of patterned nanofiber composite network (PNCN). (a) Schematic diagram, photographs, and enlarged view of PNCN. (b) Schematic illustration of the fabrication process of PNCN. (c) Scanning electron microscopy images of PNCN and enlarged view. (d) Electric field simulation of electrospinning process with flat collectors (left) and patterned collectors (right). (e) Profiles of the potential versus distance of electric fields generated using the two collectors in (d). The potential directions are shown at the left of (d) using the horizontal and vertical arrows, respectively.

1964 V, whereas the potential at the collector of the micropore fluctuates between - 1894 V and - 2000 V. These results indicate that there will be a minimum pore size for patterned electrospinning. Below this pore size, the electrospun film prepared by the patterned collector will be roughly the same as that prepared by flat collector. Thus, the flexible patterned collector fabricated by micromachining technology can achieve fine regulation of pore size.

The proposed fine patterned electrospinning technology implemented by micromachining technology can not only realize the patterning of the TPU NF film, but also possesses universality for a variety of polymers, which provides a new method for the preparation of breathable electronic skin. The parameters of patterned electrospun films based on different polymers are shown in Table S1. The SEM images of patterned electrospun films are shown in Fig. 2(a). Five different polymers, nylon (PA6), polyacrylonitrile (PAN), polyvinyl alcohol (PVA), poly(lactic-co-glycolic acid (PLGA), and TPU, can realize patterned electrospinning, which indicates that our patterned electrospinning method is universal. In the experimental operation process, PVA and PAN films are difficult to be separated from the patterned collector directly, so hydrophobic treatment was carried out on the patterned collector before transferring patterned electrospinning films. It can be seen that the patterned electrospinning films of PVA and PAN are completely peeled off without damage.

The hexagonal pattern of pores can be observed in the patterned electrospinning films of PA6, PAN, and PVA, whereas the pores in the patterned electrospun films of PLGA and TPU are closer to round. In order to explain this phenomenon, the diameters of these five polymers were counted and shown in Fig. S5. The NW

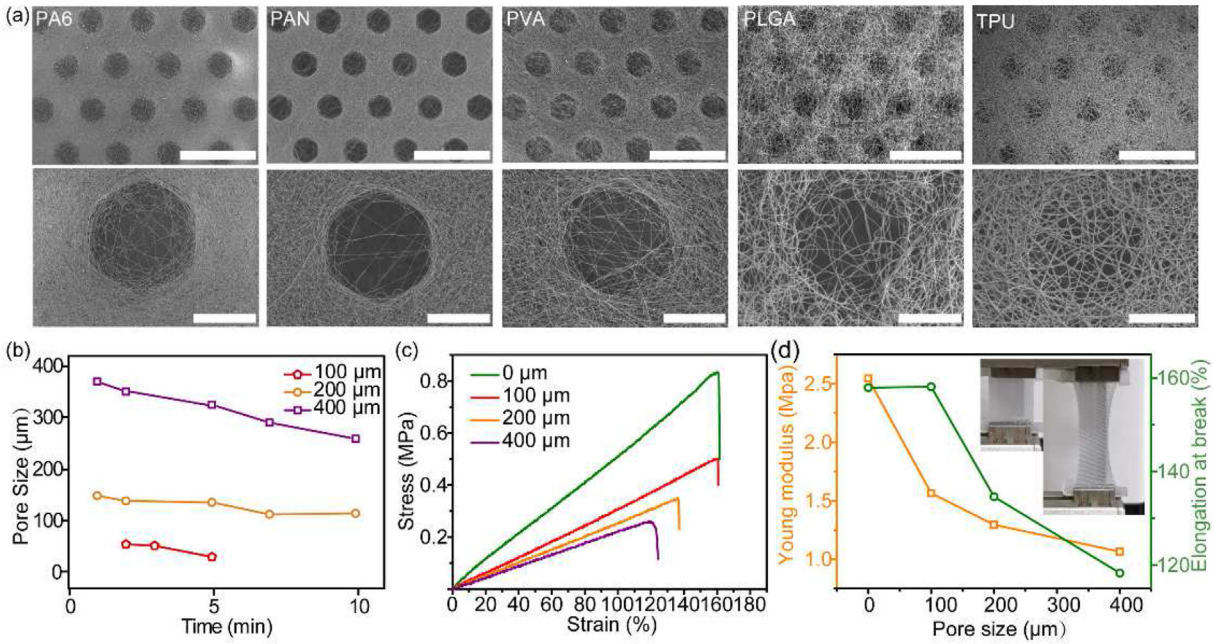

Fig. 2. Universality of patterned electrospinning technology and performance of patterned electrospinning film. (a) Universality of patterned electrospinning technology for five kinds of polymers (scale bar: 500 μm and 100 μm for the top and bottom row respectively). (b) Variation of pore size of patterned thermoplastic polyurethane nanofiber (TPU NF) films with electrospinning time. (c) Stress-strain curves of patterned TPU NF films. (d) Young's modulus and elongation at break of patterned TPU NF films with different pore sizes.

diameters of PA6, PAN, and PVA are all in the order of several hundred nanometers, compared to those of PLGA and TPU in micrometers, the potential fluctuation near the patterned collector can make them closer to the pattern of patterned collector. The hexagonal array collector with a side length of 30 μm was prepared, and the corresponding TPU NF film is shown in Fig. S6. It can be seen that there are basically no patterned pores. For TPU NFs, patterned electrospinning cannot be realized for the collector with hexagonal array with a side length less than 50 μm. However, for PA6, PAN, and PVA with smaller nanowire diameter, the minimum pore size for patterned electrospinning may be smaller.

TPU NF film possesses the advantage of outstanding stretchability and is insensitive to the humidity and temperature of electrospinning environment, so it's being chosen as the substrate for stretchable electronics. The optical photographs of I, II, and III in Fig. S7 are collector patterns with hexagonal side lengths of 50, 100, and 200 μm, respectively. Based on the patterned collector, TPU NF films with different electrospinning times were prepared. It can be seen from the Fig. S7 that with the increase in electrospinning time, the number of TPU NFs gradually increases, the film gradually thickens, and the pore size of the patterned electrospun film gradually decreases. The statistical results of pore size of patterned TPU NF films with different electrospinning times are shown in Fig. 2(b). The pore size of the patterned TPU NF films gradually decreases with the increase in electrospinning time. The reason may be that after solvent evaporation of TPU drop, TPU NFs affect the potential distribution again near the patterned collector and make the TPU NFs more concentrated inside the pore. With the electrospinning time decreasing, the pore size of the nanofiber membrane became larger. When the size of hole on the TPU NF films is large enough, Ag NWs passed through the holes during the vacuum filter process. Therefore, the number of Ag NWs on the TPU NF films reduced, leading to the bad performance of the sensor. Considering the preparation process of vacuum filter and the characteristics of patterned electrospun film, the patterned TPU NF film with an electrospinning time of 5 min was selected as the substrate of stretchable electronics. The mechanical properties of patterned TPU NF films with different pore sizes were tested and analyzed. As shown in Fig. 2(c) and (d), with the increase in pore size, the Young's modulus and elongation at break of patterned TPU NF films decrease gradually. In other words, we can control the Young's modulus of the TPU NF film by adjusting the pore size of the collector pattern.

The electromechanical performance and the stability of PNCN are studied. The resistance of PNCN with different pore sizes under applied strain is measured, as shown in Fig. 3(a). The PNCNs with different pore sizes maintain good electrical conductivity at all times under strain. The resistance change of PNCN is slow within the range of 0–40%, a relatively small strain; when the strain is greater than 60%, the resistance changes rapidly, as shown in Fig. 3(a). Among 0–200 μm pores, with the increase in pore size, the resistance changes become slower, and the stretchability increases. This is due to the decrease in Young's modulus and the increase in tensile property with the increase in pore size. Because of the large pore size, the device with 400 μm pore size cannot form the same Ag NWs density in the vacuum filtration process, so the resistance changes rapidly. As shown in Fig. 3(b), the resistance variation under 0–40% strain presents the same trend with the large strain range. The electromechanical properties of PNCN are controlled by using patterned TPU NF films as the substrate, which provide a new method for the performance modulation of stretchable electronics. In addition, we studied the electrical hysteresis properties of 0 and 200 μm holes during the strain process. The area enclosed by the change of electrical properties during the application and release of strain represents the magnitude of hysteresis. Fig. S8 shows that the hysteresis of PNCN with 200 μm holes is far less than that of 0 μm PNCN, demonstrating that the patterned PNCN can effectively reduce the hysteresis behavior of the sensor. In addition, we verified the excellence of PNCN. Compared to fibrous films of silver NWs, PNCN has a smaller and more stable response to strain, which helps in the application of stretchable electrodes (Fig. S9).

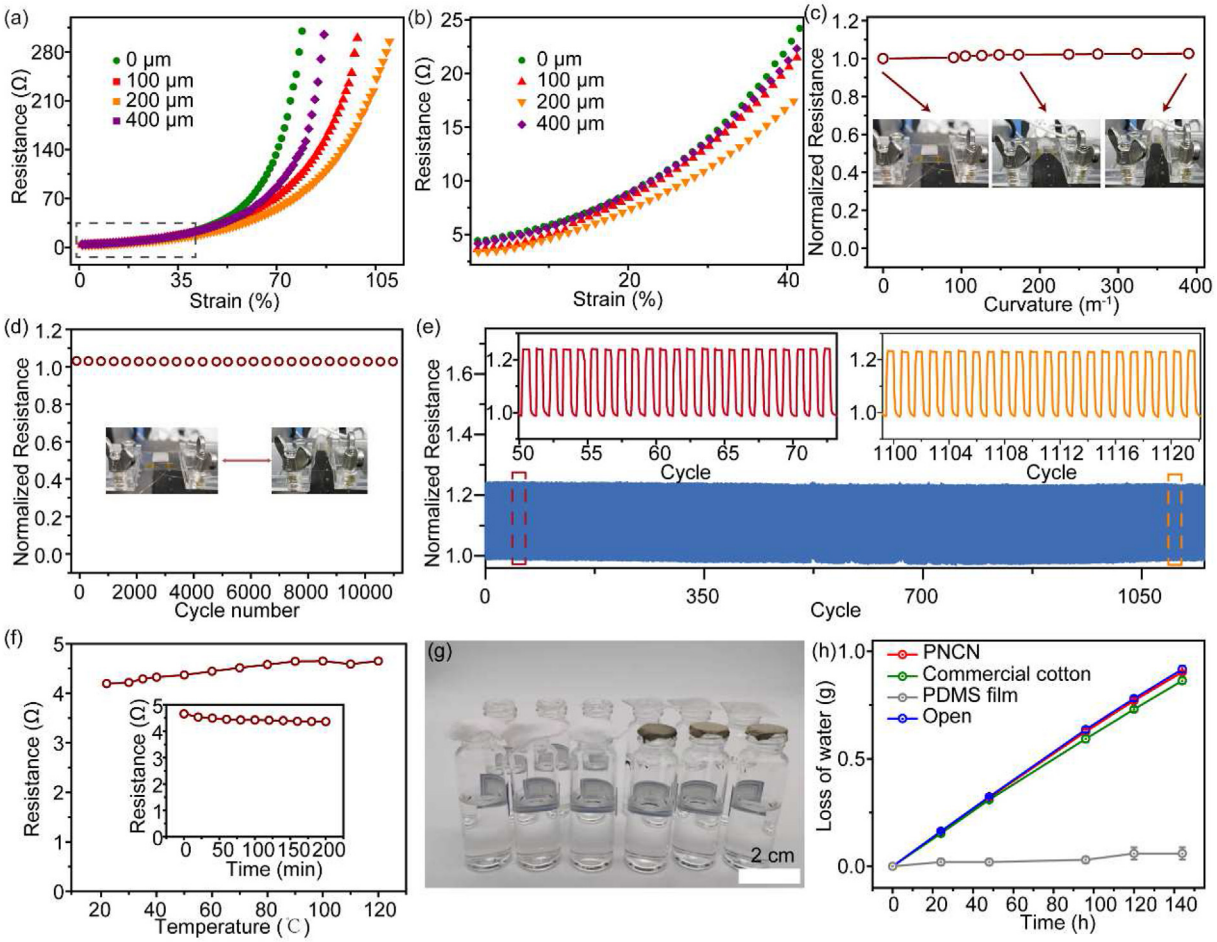

Fig. 3. Electromechanical performance, stability, and breathability of patterned nanofiber composite network (PNCN). (a) Electromechanical performance of PNCN. (b) Enlarged electromechanical performance of PNCN. (c) and (d) Bending stability of breathable and stretchable electrode. (e) Stretchable stability of breathable and stretchable electrode, and the insets show the sensor response during the beginning and the last cycles. (f) The stability of breathable and stretchable electrode under 25–120 °C. The inset shows the stability of breathable and stretchable electrodes under 120 °C for 200 min. (g) The photographs of permeability test of breathable and stretchable electrodes. (h) The loss of water in reagent bottle covered by PNCN, commercial cotton, polydimethylsiloxane, and opened reagent bottle.

The PNCNs exhibit outstanding stable conductivity under strain, especially the device with 200 μm pore size can sustain strain up to 110% and remain conductive; therefore it is a potential candidate for breathable and stretchable electrode in electronic skin field. Then, the stability of PNCN as breathable and stretchable electrode is researched. We define the normalized resistance as R/R_0, where R_0 is the resistance of the breathable electrode without strain and R is the resistance under strain. Firstly, bending stability of breathable electrode was tested. Breathable electrode was transferred to a 125-μm polyethylene glycol terephthalate(PET) substrate, and a bending curvature of 0–390 m^{-1} was applied to it. The normalized resistance of the breathable electrode is shown in Fig. 3(c). With the increase in bending curvature, the normalized resistance of the breathable electrode is almost unchanged. Under the maximum bending curvature of 390 m^{-1}, the normalized resistance of the breathable electrode only increases by 2.6%, maintaining good conductivity. When a 390 m^{-1} bending curvature is applied to the breathable electrode for more than 10,000 times, as shown in Fig. 3(d), the breathable electrode maintains a stable resistance value all the time, and after 10,000 cycles of bending test, the resistance only changes by 0.5%.

Next, 10% tensile strain was applied to the breathable electrode for over 1,000 times. As shown in Fig. 3(e), the normalized resistance of the breathable electrode increases slightly under 10% stretching but increases only by 7.9% after stretching over 1,000 times, showing good conductivity. This mainly results from the fact that the deformation is mainly borne by TPU NFs, and cracks produced on TPU-Ag NFs and Ag NWs just separate and generate a smaller displacement from TPU NFs under strain. When strain is released, cracks on TPU-Ag NFs close and Ag NWs return to their original position, so that TPU-Ag NFs and Ag NWs maintain stable conductivity. It was noted that Ag NWs with high aspect ratio possess good flexibility and connect with TPU-Ag NFs under stretching, so as to form stable conductivity. Moreover, the stability of the breathable electrode under torsion was tested; we transferred breathable electrode to a 2 × 7 cm polydimethylsiloxane (PDMS) film and applied 180° torsions to it. As shown in Fig. S10(a), after twisting the breathable electrode to 180° for more than 400 times, the normalized resistance value only increased by 4.2% at most, with good conductivity. The breathable electrode was exposed to room temperature in the atmosphere for three months, as shown in Fig. S10(b), the resistance of the breathable electrode is almost constant, which indicates that the breathable electrode is hardly oxidized in the atmosphere and shows good air stability, which is suitable for long-term electrode connection of stretchable electronics in daily life.

Human skin occasionally exposes to high temperature environment, hence the stability of breathable electrode under high temperature applications is of great significance. As shown in Fig. 3(f), when temperature was heated from room temperature to

120 °C, the resistance of the breathable electrode changes from 4.20 Ω to 4.65 Ω, showing an increase of 10.8% but maintains excellent conductivity. The resistance of the breathable electrode increases slightly with the increase in temperature, which may be due to the oxidation of Ag NWs and Ag films at high temperature. When the breathable electrode is placed at 120 °C for 200 min, as shown in the inset of Fig. 3(f), the resistance decreases slightly from 4.66 Ω to 4.36 Ω, maintaining good conductivity. This may due to the decrease in contact resistance between Ag NWs and Ag films at high temperature.

The breathability of the breathable electrode was quantitatively measured by the water loss of reagent bottles in the atmosphere. As shown in Fig. 3(g), the reagent bottles with water are covered by PNCN, commercial cotton, and PDMS, whereas a set of opened reagent bottles is set as a control group. The water loss of the PNCN is almost equivalent to that of the opened reagent bottle, and the water loss rates are 6.27 mg/h and 6.37 mg/h, respectively, which proves that PNCN possesses good water permeability, and its breathability is superior to that of the commercial cotton cloth, and far better than that of the PDMS film.

Breathable electrode shows stable conductive property to strain, bending, relative high temperature, etc. The stability of breathable electrode in practical application is also studied. In order to simulate the perspiration process and the solution that human skin may contact, the breathable electrode was soaked in deionized water, alcohol, and normal saline, and its resistance stability was tested after being dried. As shown in Fig. 4(a), the normalized resistance of breathable electrode is almost unchanged after being soaked in water, alcohol, and normal saline and dried. After the breathable electrode was soaked in normal saline for 12 h and dried, its resistance decreased slightly. The breathable electrode can not only allow the human skin sweat and breathe freely, but also maintain excellently stable conductivity, which is expected to improve the comfort of electronic skin.

Further experiments were put forward to test the stability of the breathable electrode in the actual strain application. The breathable electrode is transferred to the second joint of a finger, and the resistance value of the breathable electrode is tested and shown in Fig. 4(b). When the finger bent from the flat state to 90°, the resistance value of the breathable electrode only changes from 5.527 Ω to 6.991 Ω, which still remains at a low resistance state. When the finger is bent to 90° for more than 200 times, the normalized resistance of the breathable electrode is almost unchanged compared to that before bending, showing excellent and stable conductivity.

The breathable electrode is connected in series with a green LED lamp. A 3 V voltage is applied on the series circuit, as shown in Fig. 4(d); the LED lamp can be successfully lit up, presenting the breathable electrode a role of stable electrode. When the breathable electrode is stretched to 48% and 68% strains, respectively, the brightness of LED lamp is almost unchanged, which indicates that the breathable electrode can be applied for stretchable electrode. The breathable electrode is transferred to PET too for bending test. Similarly, the breathable electrode and the blue LED lamp form a series circuit, and a 3 V voltage is applied on the circuit, and the breathable electrode is bent upward and downward, respectively. As shown in Fig. 4(e), the LED lamp still maintains high brightness, indicating that the breathable electrode still owns excellent conductivity in the bending state, demonstrating its potential as a stretchable and bendable electrode.

The resistance of the non-PNCN changes rapidly under strain, exhibiting a sensitive response to external strain, so it can be considerably a glorious candidate for breathable resistive strain sensor. As shown in Fig. 5(a), the breathable strain sensor can realize the sensing of external strain in the range of 0–79%, and the sensitivity can reach 88 at the strain of 79%. We compared the performance of the prepared sensor to that of other ultrathin sensors, where the three parameters sensitivity, detection range, and robustness interact with each other and are very important for the performance of the sensor (Table S2). Although thin-film ultrathin sensors have high sensitivity, their crack pattern–based sensing mechanism leads to their in-general low detection range

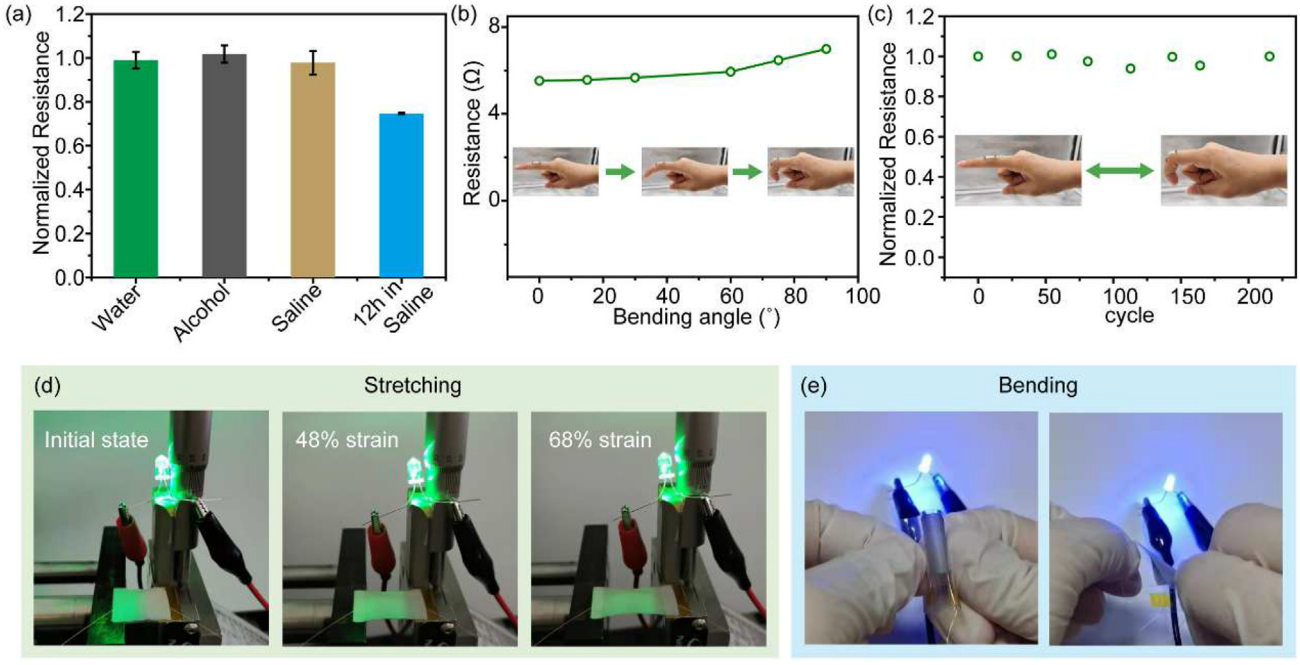

Fig. 4. Stability of breathable electrode in practical application. (a) The stability of breathable electrode after being immersed in water, alcohol, and saline. (b) The resistance of breathable electrode when transferred on finger and bent from flat state to 90°. (c) The normalized resistance of breathable electrode when bending the finger to 90° for 200 cycles. (d) Stability of the breathable electrode when in series with green LED and being stretched. (e) Stability of the breathable electrode when in series with blue LED and being bent.

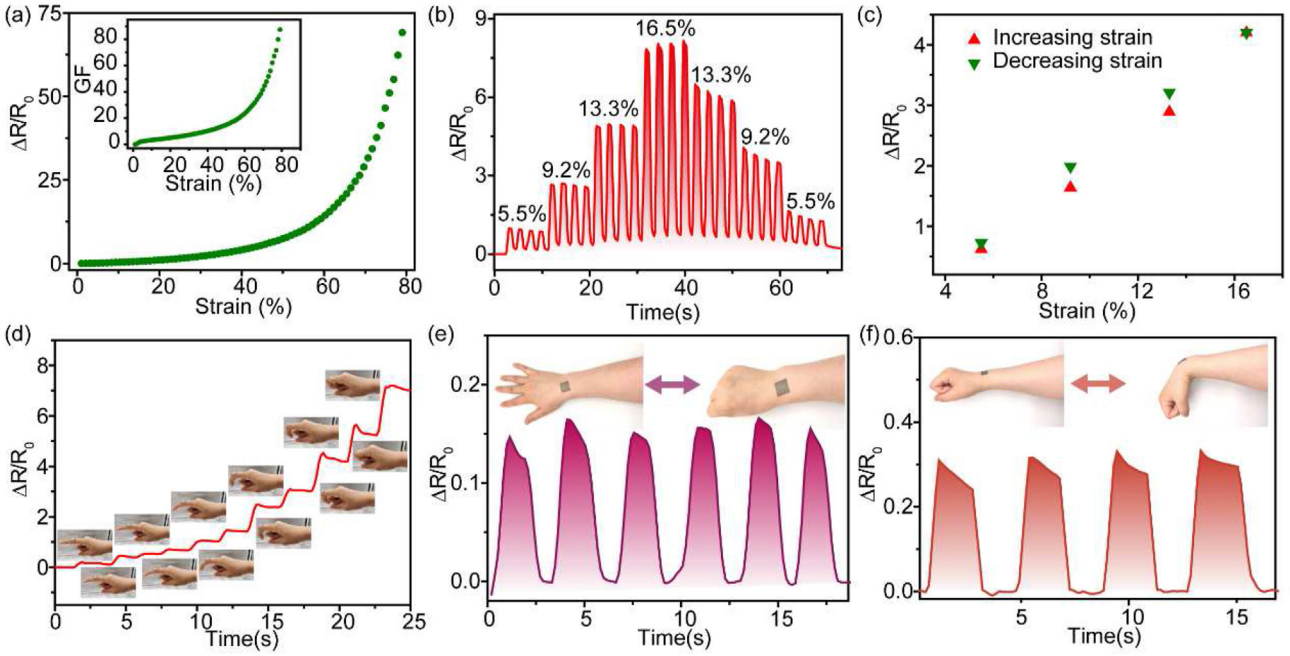

Fig. 5. Applied patterned nanofiber composite network as stretchable and breathable strain sensor and corresponding application in electronic skin. (a) The relative resistance variation and gauge factor of stretchable and breathable strain sensor. (b–c) The reversible relative resistance changes of strain sensor under increasing and decreasing strains. (d) The response of stretchable and breathable strain sensor to finger bending. (e) The response of stretchable and breathable strain sensor to make a fist. (f) The response of stretchable and breathable strain sensor to wrist bending.

and poor robustness due to the thickness of the substrate, which does not meet people's daily detection needs. Researchers decreased sensitivity of the device to ensure the range and robustness of the detection used. Figs. 3(E) and 5(A) show that we still get high sensitivity over a large detection range (80%) and that the signal remains stable over 10,000 stability tests. Result from the composite sensing layer of Ag NWs and TPU-Ag NFs shows that the breathable strain sensor not only possesses a wide detection range, but also a high sensitivity. The resilience of the breathable strain sensor was tested by gradually applying increasing strain and releasing, the relative resistance variation is basically the same, as shown in Fig. 5(b). The statistical data of Fig. 5(b) can be drawn as Fig. 5(c), which shows the good resilience of breathable strain sensor to external strain.

The ultrathin properties of the PNCN provide the breathable strain sensor the ability of being attached closely to the human skin, and the breathability promotes the wear comfort of the strain sensor. As shown in Fig. 5(d), when the finger gradually bends from straight to 120°, the breathable strain sensor responds to each bending angle. With the increase in bending angle, the relative resistance variation of the breathable strain sensor increases gradually. The breathable strain sensor can detect the finger bending signal sensitively, especially small bending angles. In addition to the angle detection of finger bending, the breathable strain sensor can be attached to any part of the skin to realize the monitoring of skin deformation. As shown in Fig. 5(e), the breathable strain sensor is transferred to the wrist, when the hand changes from the relaxed state to the clenched fist, the breathable strain sensor responds sensitively to the deformation of the wrist skin. And the breathable strain sensor responds stably and repeatedly while clenching fist six times. The breathable strain sensor can also respond to wrist bending, as shown in Fig. 5(f), a stable signal was detected in the multiple process of wrist-bending cycles.

3. Conclusion

A refined patterned electrospinning technology is proposed by fabricating a flexible patterned collector through micromachining process, and the corresponding principle is simulated. The universality of the refined patterned electrospinning technology for a variety of polymers was verified experimentally. The effects of electrospinning time and patterned pore size on the properties of electrospun films were investigated. The pore size decreased with the increase in electrospinning time, and with the increase in pore size, the elastic modulus and elongation at break of patterned TPU NFs films decrease. Stretchable ultrathin patterned TPU NFs films were selected as the substrate material for stretchable electronics. Ag NWs and films were constructed on the TPU NF substrate as the conductive layer by vacuum filtration process and magnetron sputtering technology, achieving a mean sheet resistance as low as 1.59 Ω/sq and better breathability than commercial cotton. The electromechanical properties of PNCN were controlled through modulating the pore size of patterned TPU NF film, which can be applied as a stretchable electrode that possesses stable conductivity under tension, bending, high temperature, etc. The non-PNCN presents high sensitivity to strain and a GF as high as 88 at 79% strain. The patterned electrospinning technology provides a new idea for the preparation of stretchable electronics.

In addition, in practical applications, it may be necessary to detect multiple signals simultaneously. The challenge here is that the output signals often overlap, making it difficult to decouple and distinguish them at the same time. To address this issue, we can design the substrate to isolate different mechanical stimuli and assign them to different sensors. This enables independent detection of deformation by different sensors. Advanced algorithms, such as machine learning, provide solutions for multisignal decoupling, which can be further explored with ongoing research and development.

4. Experimental Section

4.1. Fabrication of patterned TPU NF film

Firstly, the patterned collector is prepared by micromachining technology. Customed photomask is fabricated through laser direct writing process and magnetron sputtering, then patterned Ag conductive film is prepared on flexible polyethylene naphthalate two formic acid glycol ester (PEN) substrate through ultraviolet lithography and magnetron sputtering. Then the patterned Ag conductive film is utilized on flexible PEN substrate as the flexible patterned electrospinning collector, andit is put on a homemade acrylic support as the negative electrode of electrospinning. Different polymer nanofiber films were fabricated by the electrospinning equipment (Shenzhen Tong Li Tech Co. Ltd.). TPU solution was prepared by adding 20 wt% of TPU particles into dimethyl formamide (Aladdin) and then stirred well for 4 h at 60 °C. The TPU solution was sucked into a 10 ml plastic syringe and was fixed onto a syringe pump with a flow rate of 0.1 ml/h. The distance between the needle and flexible patterned collector is set as 12 cm A constant potential of 10 kV was adopted between the needle and collector. The pore size of patterned TPU NF films was controlled by the side length of a hexagonal array of patterned collectors.

4.2. Fabrication of PNCN

The TPU NF film is transferred and fixed on a 2 × 2 cm^2 PET frame using double faced adhesive tape. Then, 400 μg Ag NWs was dispersed in alcohol and was further diluted and subjected to ultrasonic dispersion for 5 min. The Ag NW was constructed on TPU NF film by vacuum filtration and was dried at 60 °C for 20 min. PNCN was finally prepared by magnetron sputtering (PVD75 Kurt J. Lesker) Ag films on Ag NW-TPU NF composite films.

4.3. Water vapor permeability test

The breathability of PNCN is characterized by the weight loss of water in a reagent bottle covered by PNCN. Thirteen g of DI water is added into 15 ml reagent bottle, and the reagent bottle is covered with PNCN, cotton, and PDMS. Three samples were prepared for each experiment, and three open reagent bottles were used as control group. All the samples were placed in a test tube stand at 25 °C and 30% humidity for 6 days. Then the weight loss of the samples was tested by an electronic scale (ME104/METTLER TOLEDO) every day.

4.4. Characterization and measurements

The morphologies of PNCN were characterized by an optical microscope (Zeiss Observer Z1) and a field-emission scanning electron microscope (SU8020 Hitachi). A four-probe resistivity measurement system (Guangzhou 4-probe Tech Co. Ltd, RTS-9) was used to measure the conductivity of PNCN. A stepping motor (XPS-2000 Newport) was introduced to add controlled strain on PNCN, and the resistance was recorded by an LCR meter (Agilent E4980A) under a sampling rate of 10 kHz.

CRediT authorship contribution statement

Jing Li and Xiaojun Pan performed the experiments, data collection, and the original manuscript writing. Rongrong Bao contributed to conceptualization, analysis, and the original manuscript writing. Yufei Zhang, Yue Liu, Chunfeng Wang, Yixin Wan and Juan Tao assisted in data analysis. Rongrong Bao and Caofeng Pan contributed to supervision. Caofeng Pan commented on and revised the manuscript, and contributed to funding acquisition, and resources.

Declaration of competing interest

The authors declare that they have no known competing financial interests or personal relationships that could have appeared to influence the work reported in this paper.

Data availability

Data will be made available on request.

Acknowledgments

The authors thank the support of Natural Science Foundation of Beijing Municipality (2222088 and Z180011), National key R&D project from Minister of Science and Technology, China (2016YFA0202703), National Natural Science Foundation of China (No. U20A20166, 61675027, 61805015 and 61804011), Shenzhen Science and Technology Program (Grant No. KQTD20170810105439418) and the Fundamental Research Funds for the Central Universities.

Appendix A. Supplementary data

Supplementary data to this article can be found online at https://doi.org/10.1016/j.mtnano.2023.100359.

References

[1] C. Pan, L. Dong, G. Zhu, S. Niu, R. Yu, Q. Yang, Y. Liu, Z.L. Wang, Nat. Photonics 7 (2013) 752–758.
[2] Y. Ling, T. An, L.W. Yap, B. Zhu, S. Gong, W. Cheng, Adv. Mater. 32 (2020) 1904664.
[3] J. Kim, A.S. Campbell, B.E.-F. de Ávila, J. Wang, Nat. Biotechnol. 37 (2019) 389–406.
[4] S. Choi, S.I. Han, D. Jung, H.J. Hwang, C. Lim, S. Bae, O.K. Park, C.M. Tschabrunn, M. Lee, S.Y. Bae, J.W. Yu, J.H. Ryu, S.-W. Lee, K. Park, P.M. Kang, W.B. Lee, R. Nezafat, T. Hyeon, D.-H. Kim, Nat. Nanotechnol. 13 (2018) 1048–1056.
[5] S. Soltanian, R. Rahmanian, B. Gholamkhass, N.M. Kiasari, F. Ko, P. Servati, Adv. Energy Mater. 3 (2013) 1332–1337.
[6] M.A.H. Khondoker, A. Ostashek, D. Sameoto, Adv. Eng. Mater. 21 (2019) 1900060.
[7] P. Wu, J. Fu, Y. Xu, Y. He, Acs Appl Mater Inter 14 (2022) 13458–13467.
[8] W. Lee, H. Kim, I. Kang, H. Park, J. Jung, H. Lee, H. Park, J.S. Park, J.M. Yuk, S. Ryu, J.-W. Jeong, J. Kang, Science 378 (2022) 637–641.
[9] J. Zhang, B. Ma, G. Chen, Y. Chen, C. Xu, Q. Hao, C. Zhao, H. Liu, Acs Appl Mater Inter 14 (2022) 53405–53412.
[10] M. Tavakoli, M.H. Malakooti, H. Paisana, Y. Ohm, D. Green Marques, P. Alhais Lopes, A.P. Piedade, A.T. de Almeida, C. Majidi, Adv. Mater. 30 (2018) 1801852.
[11] A.F. Silva, H. Paisana, T. Fernandes, J. Góis, A. Serra, J.F.J. Coelho, A.T. de Almeida, C. Majidi, M. Tavakoli, Adv Mater Technol-Us 5 (2020) 2000343.
[12] M.-g. Kim, D.K. Brown, O. Brand, Nat. Commun. 11 (2020) 1002.
[13] S. Han, K. Kim, S.Y. Lee, S. Moon, J.-Y. Lee, Adv. Mater. 35 (2023) 2210112.
[14] Y.J. Fan, P.T. Yu, F. Liang, X. Li, H.Y. Li, L. Liu, J.W. Cao, X.J. Zhao, Z.L. Wang, G. Zhu, Nanoscale 12 (2020) 16053–16062.
[15] I. Kim, K. Woo, Z. Zhong, P. Ko, Y. Jang, M. Jung, J. Jo, S. Kwon, S.-H. Lee, S. Lee, H. Youn, J. Moon, Nanoscale 10 (2018) 7890–7897.
[16] G. Ge, Q. Wang, Y.-Z. Zhang, H.N. Alshareef, X. Dong, Adv. Funct. Mater. 31 (2021) 2107437.
[17] Y. Wang, Z. Wang, Z. Wang, T. Xiong, P.P. Shum, L. Wei, Advanced Electronic Materials 9 (2023) 2201194.
[18] R.L. Truby, J.A. Lewis, Nature 540 (2016) 371–378.
[19] W. Gao, S. Emaminejad, H.Y.Y. Nyein, S. Challa, K. Chen, A. Peck, H.M. Fahad, H. Ota, H. Shiraki, D. Kiriya, D.-H. Lien, G.A. Brooks, R.W. Davis, A. Javey, Nature 529 (2016) 509–514.
[20] Z. Jiang, M.O.G. Nayeem, K. Fukuda, S. Ding, H. Jin, T. Yokota, D. Inoue, D. Hashizume, T. Someya, Adv. Mater. 31 (2019) 1903446.
[21] L. Liu, H.Y. Li, Y.J. Fan, Y.H. Chen, S.Y. Kuang, Z.B. Li, Z.L. Wang, G. Zhu, Small 15 (2019) 1900755.
[22] Y. Wang, J. Wang, S. Cao, D. Kong, J. Mater. Chem. C 7 (2019) 9748–9755.
[23] Q. Gao, B.A.F. Kopera, J. Zhu, X. Liao, C. Gao, M. Retsch, S. Agarwal, A. Greiner, Adv. Funct. Mater. 30 (2020) 1907555.

[24] S. Lee, D. Sasaki, D. Kim, M. Mori, T. Yokota, H. Lee, S. Park, K. Fukuda, M. Sekino, K. Matsuura, T. Shimizu, T. Someya, Nat. Nanotechnol. 14 (2019) 156–160.
[25] A. Miyamoto, S. Lee, N.F. Cooray, S. Lee, M. Mori, N. Matsuhisa, H. Jin, L. Yoda, T. Yokota, A. Itoh, M. Sekino, H. Kawasaki, T. Ebihara, M. Amagai, T. Someya, Nat. Nanotechnol. 12 (2017) 907–913.
[26] C. Tan, Z. Dong, Y. Li, H. Zhao, X. Huang, Z. Zhou, J.-W. Jiang, Y.-Z. Long, P. Jiang, T.-Y. Zhang, B. Sun, Nat. Commun. 11 (2020) 3530.
[27] W. Yang, N.-W. Li, S. Zhao, Z. Yuan, J. Wang, X. Du, B. Wang, R. Cao, X. Li, W. Xu, Z.L. Wang, C. Li, Advanced Materials Technologies 3 (2018) 1700241.
[28] N. Liu, G. Fang, J. Wan, H. Zhou, H. Long, X. Zhao, J. Mater. Chem. 21 (2011) 18962–18966.
[29] X. Li, Y.J. Fan, H.Y. Li, J.W. Cao, Y.C. Xiao, Y. Wang, F. Liang, H.L. Wang, Y. Jiang, Z.L. Wang, G. Zhu, ACS Nano 14 (2020) 9605–9612.
[30] J. Cao, Z. Cheng, L. Kang, M. Lin, L. Han, RSC Adv. 10 (2020) 20155–20161.
[31] C. Vaquette, J.J. Cooper-White, Acta Biomater. 7 (2011) 2544–2557.
[32] X. Wang, F. Lv, T. Li, Y. Han, Z. Yi, M. Liu, J. Chang, C. Wu, ACS Nano 13 (2019) 3740, 3740.
[33] S. Nedjari, S. Eap, A. Hébraud, C.R. Wittmer, N. Benkirane-Jessel, G. Schlatter, Macromol. Biosci. 14 (2014) 1580–1589.
[34] D. Zhang, J. Chang, Adv. Mater. 19 (2007) 3664–3667.
[35] D. Li, Y. Wang, Y. Xia, Adv. Mater. 16 (2004) 361–366.
[36] Y. Wu, Z. Dong, S. Wilson, R.L. Clark, Polymer 51 (2010) 3244–3248.
[37] M. Kakunuri, N.D. Wanasekara, C.S. Sharma, M. Khandelwal, S.J. Eichhorn, J. Appl. Polym. Sci. 134 (2017).
[38] C.M. Rogers, G.E. Morris, T.W.A. Gould, R. Bail, S. Toumpaniari, H. Harrington, J.E. Dixon, K.M. Shakesheff, J. Segal, F.R.A.J. Rose, Biofabrication 6 (2014) 035003.
[39] S. Zhao, Q. Zhou, Y.-Z. Long, G.-H. Sun, Y. Zhang, Nanoscale 5 (2013) 4993–5000.
[40] S. Zhang, H. Liu, N. Tang, J. Ge, J. Yu, B. Ding, Nat. Commun. 10 (2019) 1458.